Second-Sound Velocity and Superfluid Density in ^{4}He under Pressure near T_λ

Dennis S. Greywall and Guenter Ahlers
Bell Laboratories, Murray Hill, New Jersey 07974
(Received 24 January 1973)

The velocity of second sound was measured in superfluid ^{4}He between vapor pressure and the melting pressure for $T \geq 1.6$ K. Particular emphasis was given to the temperature region near T_λ with $2 \times 10^{-5} \lesssim \epsilon \equiv 1 - T/T_\lambda(P) \lesssim 10^{-2}$. Using these results, other existing thermodynamic information, and linear two-fluid hydrodynamics, the superfluid fraction ρ_s/ρ was determined. The higher-pressure data at small ϵ revealed that ρ_s/ρ along isobars cannot be described by a pure power law in ϵ. Instead, singular corrections to the leading power-law term exist which are much larger than of order ϵ. Therefore, the results were fitted to the expression $\rho_s/\rho = k(P)\epsilon^\zeta[1 + a(P)\epsilon^y]$. They yielded $0.66 \lesssim \zeta \lesssim 0.68$ and $0.4 \lesssim y \lesssim 0.6$, independent of the pressure P. These results for the exponents, and the existence of singular corrections, are consistent with scaling, universality, and recent explicit calculations.

I. INTRODUCTION

We report in this paper the results of precision measurements of the second-sound velocity u_2 in He II. Our data are for $T \geq 1.6$ K and for the entire pressure range from saturated vapor pressure to the freezing pressure. This work was motivated primarily by the possibility of testing theoretical predictions about critical phenomena.[1-9] We therefore obtained particularly detailed results over the range $2\times10^{-5} \lesssim \epsilon \lesssim 10^{-2}$, where $\epsilon \equiv 1 - T/T_\lambda(P)$ and T_λ is the superfluid transition temperature.

For the study of critical phenomena in He II near T_λ, it would be desirable to know the behavior of the order parameter $|\psi|$. This order parameter is proportional to the number of atoms in the zero-momentum state,[10] and has not yet been accessible to direct measurement. A closely related quantity,[5] however, is the superfluid fraction ρ_s/ρ. This variable is a hydrodynamic parameter,[11] and is related to several experimentally accessible quantities through the predictions[11] of linear two-fluid hydrodynamics. These predictions are believed to be exact. They have indeed been verified at vapor pressure and near T_λ by several diverse, precise experiments[12-16] which all yielded, within the small experimental errors, the same ρ_s/ρ (see Sec. III B). We will use one of these predictions, to be given in Eq. (6), to derive ρ_s/ρ from the known thermodynamic parameters near T_λ and from our measured second-sound velocity.

Near critical points, the thermodynamic, hydrodynamic, and transport properties are usually written as power laws in parameters which describe the "distance" from the critical point.[1,17] For the superfluid transition only the dependence upon the distance ϵ along the temperature axis is accessible to experiment because the field conjugate to the order parameter cannot be varied in the laboratory. We can define an exponent ζ for ρ_s/ρ by the asymptotic proportionality $\rho_s/\rho \sim \epsilon^\zeta$. This exponent is related by the predictions of scaling[2,3,5] to the exponent α', which characterizes the singularity in the heat capacity at constant pressure C_p. One of the major purposes of this work was to provide data for ρ_s/ρ which could be used, together with the already known results[18-20] for C_p, to test this scaling relation at all pressures at which the transition exists. The results for ζ and α' are within their errors in agreement with the predicted scaling law. In addition, it is expected on the basis of universality arguments[6] and explicit calculations[7,8] that the scaling parameters near T_λ should be independent of the pressure. In the case of C_p, this universality appears to be obeyed by the exponent, but seems to be violated by the ratio of the amplitude above T_λ to that below T_λ.[20] Contrary to theory,[8] this ratio depends upon the pressure. In agreement with theory, we find from ρ_s/ρ that the exponent ζ is within our errors independent of P.

Although there is no reason to assume that the leading singular power-law contribution to various properties near critical points is the only singularity,[17] experimental measurements at small ϵ have usually been interpreted in terms of pure power laws. Implicit in such interpretations is the assumption that other contributions besides the leading term are regular functions of the temperature, and therefore of order ϵ and small for small ϵ. Our results for ρ_s/ρ at the higher pressures could not be represented within their random or systematic errors by a pure power law even when ϵ was small. In our interpretation of ρ_s/ρ we therefore had to invoke singular contributions which were of higher order than the leading singularity, and which were appreciable even for small ϵ. We wrote these correction terms also as a power law. Their presence greatly increases the

probable errors for all parameters derived from a particular set of data. Within these larger errors, and again in agreement with universality arguments[6] and explicit calculations,[9] the correction exponent [to be defined explicitly in Eq. (11)] which we derived from the data is independent of P. It has a value which agrees well with a recent calculation.[9]

It is interesting to note that the thermal conductivity just above T_λ also cannot be represented by a pure power law, or a power law with logarithmic corrections[19] suggested by theory.[21] Less direct evidence for singular corrections to the asymptotic behavior also exists for C_p near T_λ.[18-20] It appears that pure power laws have far too frequently been used to derive exponents with deceivingly small statistical errors from experimental measurements.

Preliminary reports[22,23] of portions of this work have previously been published. In Sec. II of this paper we present details of the experimental techniques. We give more complete results for the second-sound velocity and the superfluid density in Sec. III. In this section we also compare the results for ρ_s/ρ at vapor pressure with measurements by others[12-16] which are based upon different predictions of two-fluid hydrodynamics. A detailed comparison with theory is given in Sec. IV. The results of this work are summarized in Sec. V.

II. EXPERIMENT

A. General Method

The second-sound velocity was determined as a function of $T_\lambda - T$ by measuring the frequency of the plane-wave resonant modes of a cylindrical resonator. In general, the resonant frequencies f of a cylindrical cavity are given by[24]

$$f_{pmn} = \tfrac{1}{2}u[(p/l)^2 + (\alpha_{mn}/r)^2]^{1/2}, \quad (1)$$

where u is the sound velocity, p (an integer) the mode number (harmonic), and where l and r are the length and radius of the cavity, respectively. The pure numbers α_{mn} are solutions of $d[J_m(\pi\alpha)]/d\alpha = 0$, where $J_m(\pi\alpha)$ is a Bessel function of the first kind. Thus, for the plane-wave modes, which have $\alpha_{00} = 0$, the sound velocity is given by the familiar relation

$$u_2 = 2lf/p. \quad (2)$$

Sometimes the resonances with m and n not equal to zero were also excited in our cavity, but the plane-wave resonances could always be easily distinguished and were well separated from these "Bessel-function" resonances.

B. Resonator and Pressure Cell

A schematic drawing of the pressure cell which contained the second-sound resonator is shown in Fig. 1. The cell consisted of a thin-walled (0.75 mm) stainless-steel cylinder terminated at each end by heavy copper end caps. These caps were sealed with 0.9-mm indium O rings to brass flanges which had been hard soldered onto the cylinder. Two electrical leads from the resonator passed out of the cell through epoxy-filled 3.2-mm-diameter holes drilled through the center of each of the end caps. The helium sample (≈ 5.3 cm^3) entered the cell through a 0.2-mm-i.d., 0.4-mm-o.d. stainless-steel capillary passing through the top end cap. A heat switch contact post, wrapped with a 5-kΩ Karma-wire heater, was also hard soldered to this cap.

The main thermometer consisted of a bank of five 56-Ω Allen Bradley carbon resistors connected in series. The resistors were first ground flat on one side to improve the thermal contact and then attached to the bottom end cap of the cell with GE 7031 varnish. A thin sheet of Mylar provided electrical insulation. In order to measure temperature gradients across the cell, a differential thermometer consisting of a pair of thermometers identical to the main thermometer was mounted on the top and bottom of the cell. In addition, a calibrated germanium thermometer was attached to the bottom of the cell. The ^{3}He vapor-pressure bulb shown in Fig. 1 was not used in the present experiment.

Our method of generating second sound is in principle the same as that used first by Williams *et al.*,[25] and by Sherlock and Edwards.[26] An exploded diagram of the second-sound resonator is shown in Fig. 2. This resonator consisted of a cylindrical cavity, was constructed mainly of stainless steel, and had nominal dimensions of 1-cm diameter and 1-cm height. The resonator body ends were ground flat and parallel to within 0.005 mm, and were covered by stretched Nuclepore filter[27] membranes. The nominal hole size of the filter pores was 1 μm. Each membrane was held in place by an annular stainless-steel clamping ring which was drawn tightly against the body with six No. 0-80 screws. The inside surface of each of the membranes was covered with a thin layer of evaporated gold which was electrically grounded to the cell body. The Nuclepore membranes were the vibrating elements of the superleak-condenser transducers. The backing plates shown in Fig. 2 were electrically insulated and centered inside the clamping rings by the Teflon sleeves. They served as the stationary elements of the condenser transducers. The backing plates were pressed against the cell body with phosphor-bronze coil springs epoxied into the pressure cell end caps. These springs also served as electrical contacts. Beryllium-copper wave springs, which were attached to the clamping rings, electrically grounded the reso-

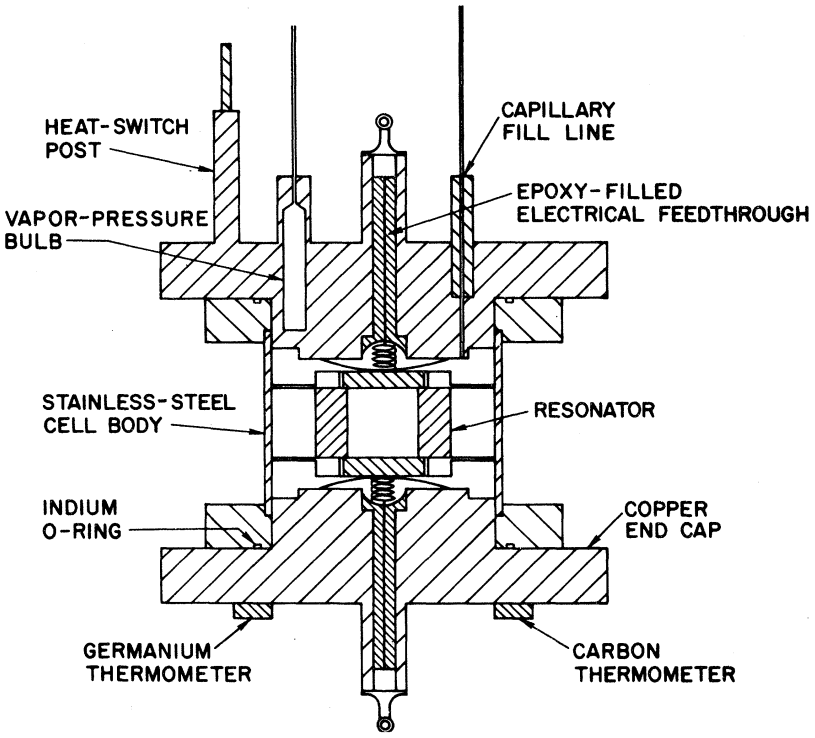

FIG. 1. Schematic diagram of the pressure cell.

nator and positioned it firmly near the center of the pressure cell. The sample entered the resonator by flowing around the Teflon sleeves and through the holes in the transducer membranes.

Before deciding on this particular resonator design, many variations were tested. Among these were flatter pancake-shaped resonators which had the advantage of smaller gravity effects. However, it was found impossible to excite only plane-wave modes, and we were forced to the taller-shaped resonators where the "Bessel-function" modes differ more in frequency from the desired resonances. Tests of rough and smooth backing plates lead us to prefer polished backing plates with a very thin coating of Krylon.[28] This insulating layer was found to be necessary due to the conduction bridges through some of the holes in the transducer membrane formed by the evaporated gold. We observed that the signals obtained using 1-μm Nuclepore were cleaner than those obtained using larger-pore-size Nuclepore and extremely superior to the signals obtained with the thicker Millipore filters used by others.[25,26]

C. Cryostat

To provide adequate thermal isolation, the pressure cell was suspended with heavy cotton strings inside the brass vacuum can which is shown schematically in Fig. 3. The can was in turn situated in a liquid-helium bath pumped to approximately 1.4 K. Aside from the addition of a ^{3}He platform, a mechanical heat switch, and a pair of stainless-steel coaxial leads, the cryostat was very similar to a calorimeter described in detail elsewhere.[18]

The ^{3}He stage was added to the cryostat to increase its flexibility. In the present work, however, it was not necessary to achieve temperatures below 1.4 K. Therefore the ^{3}He chamber was partially filled with ^{4}He which thermally shorted the "^{3}He platform" to the bath by film flow.

D. Thermometry

The temperature was determined using an ac-bridge technique.[29] The bridge ratio R was the

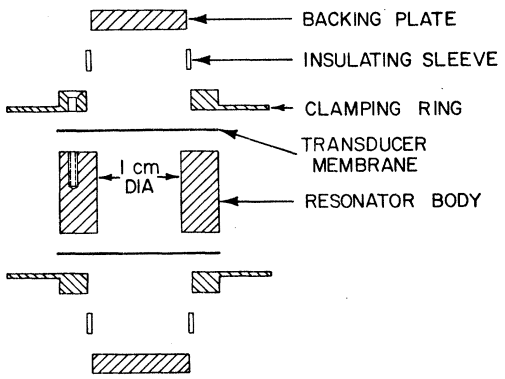

FIG. 2. Exploded cross-sectional diagram of the resonator.

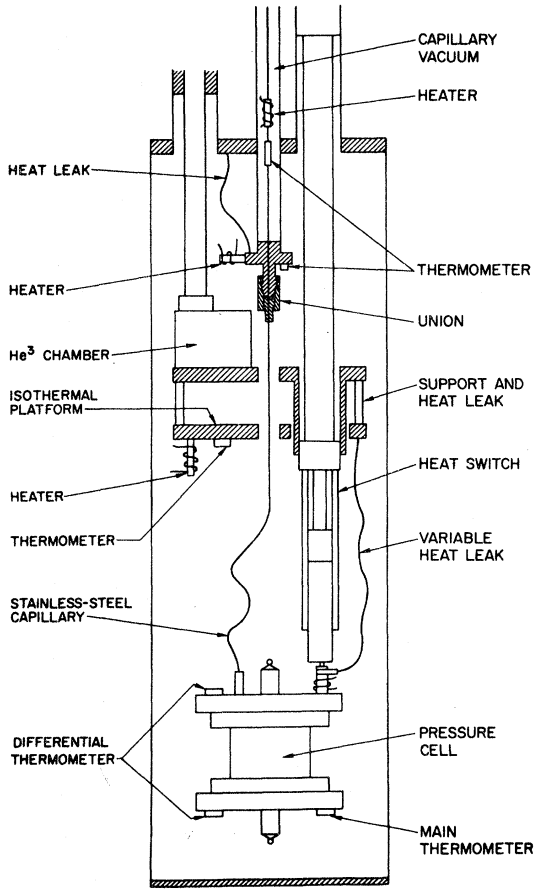

FIG. 3. Schematic diagram of the cryostat.

ratio between the strongly temperature-dependent resistance of the carbon thermometer and a nearly constant reference resistance. The reference was a nominally 10-kΩ Karma-wire-wound resistor mounted on the cell body. Having the reference resistor directly on the cell rather than at room temperature has two main advantages. First, its weak temperature dependence is automatically in the calibration, eliminating the need to maintain it at constant temperature. Second, the Johnson noise voltage originating in the reference resistor is reduced by an order of magnitude.

Temperature gradients across the vertical length of the cell were monitored with a second ac-bridge circuit which gave the resistance ratio of a pair of nearly identical carbon thermometers mounted one each on the top and bottom of the cell. Of course, below T_λ this gradient was negligible, and the bridge ratio was essentially temperature independent. Above T_λ the thermal conductivity of He I and of the stainless-steel cell body was small and the slight difference in heat input to the top and bottom of the cell caused easily measurable gradients. The abrupt change in the ratio as the transition was crossed was used to determine R_λ of the main thermometer. Usually, small drift rates of the order of 1 μK/min were used for this purpose. A sharp change in the warming drift rate monitored by the main thermometer also occurred at T_λ. The transition temperature could be determined with a precision of better than 0.2 μK. Because the main-bridge ratio R_λ at the transition was slightly time dependent[18] ($dR_\lambda/dt \approx 6\times10^{-8}$ min^{-1}), it was necessary to make frequent measurements of R_λ. A linear interpolation in time was then used to determine $R_\lambda(t)$. The time dependence of R_λ, however, was not strictly linear and may have been affected somewhat by small density changes in the sample which could have been caused by nonequilibrium conditions in the fill capillary. We estimate that the interpolation may be responsible for uncertainties in T_λ of ±1 μK.

The main-bridge ratio was calibrated with a precision of 10^{-4} K against a germanium thermometer which was previously calibrated against the 1958 ^{4}He vapor pressure scale.[30] The calibration points were used to determine values of $F(R)\equiv\delta T/\delta R$ which over the narrow range in T involved in the measurement near T_λ were fitted to a quadratic function in R. Values of $\Delta T\equiv T_\lambda - T$ were then obtained from $\Delta R\equiv R_\lambda - R$ by

$$\Delta T = \Delta R F(\bar{R}),$$

where $\bar{R}\equiv R_\lambda + \frac{1}{2}\Delta R$. With a peak-to-peak noise in R of less than 0.25 ppm it was possible to resolve 1.5×10^{-7} K (20% of the peak-to-peak noise).

E. Electronics

A block diagram of the electronics used in determining the resonant frequencies of the second sound is shown in Fig. 4. It is similar to the system used by Barmatz and Rudnick[31] in their measurements of the first-sound velocity near T_λ. The center of the system is the wave analyzer[32] which was used to both excite and detect the resonances. In the tracking-generator mode of operation the output sine-wave signal is always in tune with the narrow-bandwidth window filter of the analyzer. Thus by slowly mechanically[33] sweeping the frequency of the analyzer, the resonances could be mapped out as a function of frequency. It was also possible, because of the rapidly changing second-sound velocity near T_λ, to hold the frequency fixed and map out the resonances as a function of temperature. Since the unbiased drive transducer[34] generated sound waves of twice the driving frequency, it was necessary to halve the frequency at some point in the loop in order to return a signal of the original frequency to the analyzer. Therefore the input to the resonator was interrupted with a frequency divider which had a constant-amplitude square-wave output. This square wave

was used to trigger a phase-locked oscillator[35] which provided a variable-amplitude low-distortion sine wave of frequency $\frac{1}{2}f$. The signal, detected with the biased (60 V) receiving transducer, was amplified[36] by a factor of 10^4 and then fed back to the analyzer. The analog output of the analyzer, which was proportional to the amplitude of the signal, was recorded on a two-pen chart recorder along with the driving frequency. The resonance frequencies, which varied between 2 and 12 kHz, could be read from the chart to within 1 Hz.

F. Procedure and Tests

With the Dewar at room temperature, the pressure cell was flushed several times with purified helium gas and then pressurized to approximately 15 bar. The cell was then cooled to liquid-nitrogen temperatures, using nitrogen exchange gas in the brass can. Next, the exchange gas was pumped from the can and the liquid nitrogen in the main bath replaced with liquid helium. At this point sufficient ^{4}He gas was let into the "^{3}He" chamber to allow condensation. With the bath pumped to below the transition temperature, the ^{3}He platform cooled via film flow and liquid reflux to the bath temperature. Using the heat switch, the cell could next be cooled quickly to below the λ temperature. Additional purified helium gas[37] was then condensed into the cell by maintaining an external input pressure

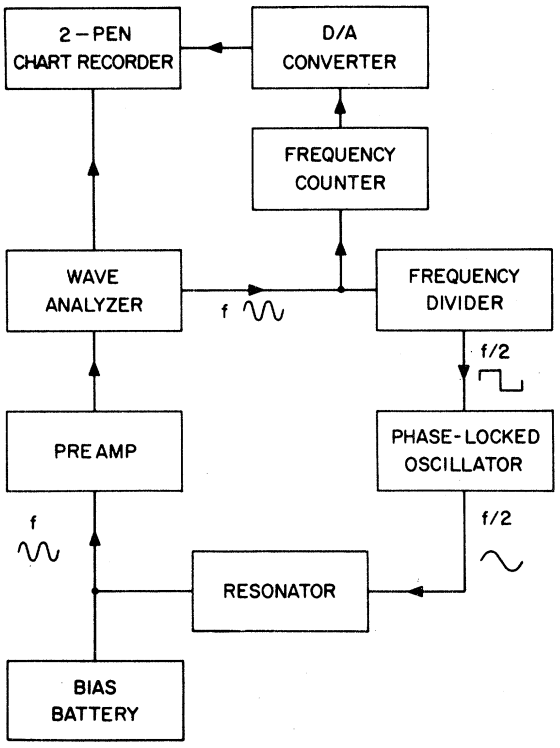

FIG. 4. Block diagram of the electronic circuitry.

of approximately 2.5 bar. This sample input rate did not warm the cell above T_λ and allowed it to be filled within one hour. A sharp increase in the pressure indicated that the liquid level had reached the capillary. If measurements were to be made at vapor pressure, part of the liquid was now pumped away to ensure that the liquid-vapor interface was located within the cell. If measurements were to be made under pressure, additional helium was admitted to the cell until the desired working pressure was reached. Several hours were now required for the establishment of a steady-state temperature and density gradient along the capillary. With the λ temperature stable, the cell temperature was held within a few μK of $T_\lambda(P)$ while the pressure P_λ was recorded.[37] A valve in the capillary line mounted at the top of the cryostat was then closed; the helium in the cell was thereafter confined to constant volume.

Before measurements were started, the cell temperature was lowered to approximately $T_\lambda - 0.1$ K and then held constant to within a few tenths of a μK while several resonances were swept out as a function of frequency. A typical example of a small section of such a frequency sweep is shown in Fig. 5. In addition to one of the plane-wave modes with $m=n=0$, one of the "Bessel-function" modes with $m=0$, $n=1$ is also observed here. However, it can be seen that the $(p00)$ mode is well separated from the $(p01)$ mode. The fundamental frequency is given by the difference between successive plane-wave resonance frequencies, and was used to label the recorded resonances according to harmonic number. A particular resonance—often the 15th harmonic—was then singled out and followed in toward the transition temperature. The procedure was to map out this resonance at constant temperature by sweeping from above to below the resonance frequency. The temperature and resonance frequency were recorded, and then the temperature was increased with the frequency fixed. The temperature step and corresponding velocity change were large enough to shift the resonance frequency to below the temporarily fixed frequency of the wave analyzer. Thus, as the cell was warmed, the same resonance was swept out at several discrete constant temperatures. Occasionally, as a test of our procedure the harmonic number was redetermined by a frequency sweep over a wider range. The same resonance was usually followed to within $\frac{1}{2}$ mK of T_λ. The only interruptions in this procedure were the regular excursions to T_λ which were necessary to keep track of the slow drift in R_λ. To make measurements nearer T_λ than $\frac{1}{2}$ mK it was found more convenient, because of the small rapidly changing second-sound velocity, to fix the frequency at approximately 2 kHz and drift in temperature at rates of approxi-

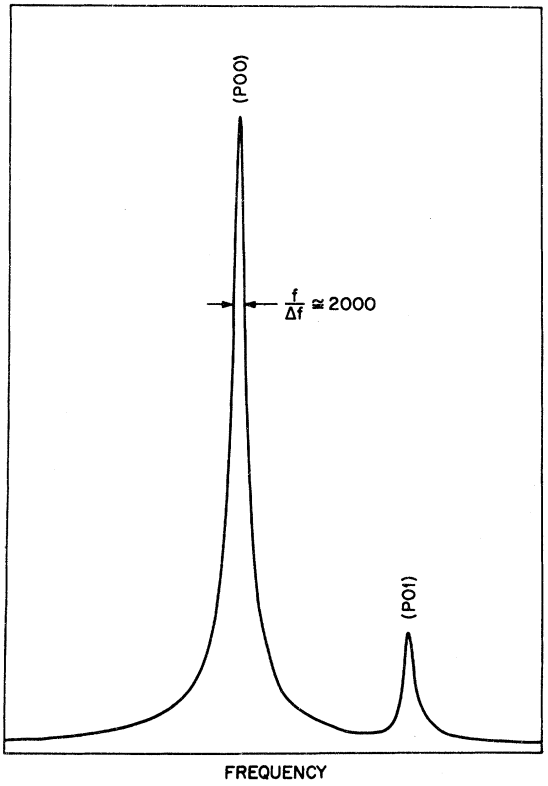

FIG. 5. Examples of typical second-sound resonances recorded at approximately 0.1 K below T_λ. The larger peak corresponds to a plane-wave resonance, and the smaller one to a "Bessel-function-mode" resonance. The definitions of the elements of the label (pmn) are given by Eq. (1). At temperatures very near T_λ, $f/\Delta f$ decreased to about 100.

mately 5 μK/min towards T_λ. Occasional comparisons with velocities measured by sweeping the frequency at constant temperature showed that the drift method did not introduce any detectable errors.

Very near T_λ, when the frequency was held constant and the temperature permitted to drift, harmonics as high as the 90th plane-wave mode were recorded. These high modes had a second-sound wavelength of approximately 200 μm, which is still large compared with the coherence length ξ. When $T_\lambda - T$ was sufficiently small, ξ became as large as 1 μm. At these temperatures, it was approximately equal to the size of the holes in the transducer membrane, and a second-sound signal was no longer detectable.

As T_λ is approached, the amount of first sound generated by the superleak transducers increases. This can be demonstrated by considering the idealized boundary conditions at the diaphram.[26] As a check against the possibility that this could affect our second-sound resonance, pulse-echo velocity measurements were carried out near T_λ at 12.13 bar. Although the uncertainty in these results was larger than that in the resonance method, the two sets of data agreed within a few tenths of one percent.

We searched for possible nonlinear effects by varying the transducer driving voltage between 1 and 12 V rms. No shift in the peak frequency was detected, although the highest driving voltages tended to produce some resonance-shape distortion. The 4-V rms driving voltage used in collecting data provided a strong signal with no measurable distortion.

We searched for a possible dependence of our measured velocity upon the frequency, but within our resolution no dispersion was detected. The measured f/p of the plane-wave modes was independent of the harmonic to within less than 0.1% for frequencies between 1.5 and 9.5 kHz when $T_\lambda - T$ was $\approx 1.5\times10^{-3}$ K.

Finally, as a check of our complete system, measurements were made of the second-sound velocity far from the transition ($T_\lambda - T \gtrsim 10^{-2}$ K) and at pressures up to 26 bar. These results are given in Table I and are represented graphically by the smooth solid lines in Fig. 6. The isotherms between 1.6 and 1.9 K are seen to be in good agreement with the results of Peshkov and Zinov'eva.[38] Their velocities were obtained using a glass reso-

TABLE I. Second-sound velocities at temperatures far from T_λ.

T(K)	P (bar)	u_2 (m/sec)
1.600	SVP	20.38
	2.11	19.77
	7.71	18.45
	10.36	17.90
	15.16	16.91
	20.33	15.73
	26.26	14.00
1.700	SVP	20.36
	2.11	19.72
	10.19	17.59
	14.89	16.34
	20.33	14.59
	26.24	11.83
1.800	SVP	19.89
	2.11	19.19
	10.22	16.62
	15.15	14.78
	20.32	12.19
1.900	SVP	18.78
	2.11	17.97
	6.09	16.38
	10.22	14.58
	15.14	11.71
	20.29	6.13

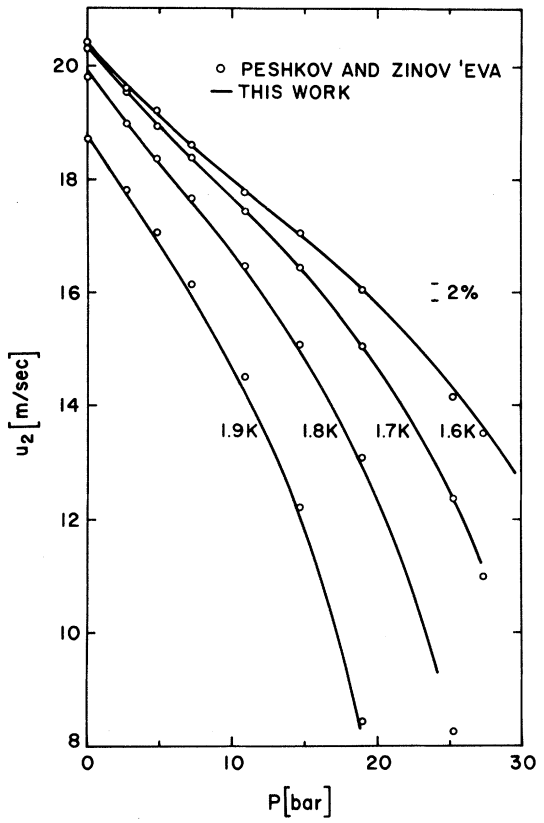

FIG. 6. Second-sound velocity as a function of pressure. The solid curves correspond to the isotherms determined by the data listed in Table I. The open circles were taken from a plot of u_2 data published in Ref. 38.

nator, 13 cm long, in which second sound was excited and detected by a heater and thermometer, respectively. The present results also are consistent within allowed experimental errors with the second-sound velocities measured by Maurer and Herlin,[39] although these results tend to be systematically higher than ours by 2 or 3%. The results of Ref. 39 were obtained by a heater-pulse technique in a cell which was 4 cm long.

III. RESULTS

A. Second-Sound Velocity

The experimental data measured under saturated vapor pressure (SVP) and along five isochores consisted of pairs of values of the fundamental plane-wave resonant frequency f/p, and the temperature difference $T_{\lambda b} - T$. $T_{\lambda b}$ is that temperature at which, upon slowly warming, we first detected a vertical temperature gradient along the cell (see Sec. II D) corresponding to the onset of thermal resistance in the liquid. Since the slope of the λ line $(\partial P/\partial T)_\lambda$ is negative, the gravity-induced pressure gradient causes a lower transition temperature at the bottom of the cell than at the top.[29] Thus $T_{\lambda b}$ is the λ temperature at the bottom of the cell. Using the derivative $(\partial P/\partial T)_\lambda$,[40] the gravitational acceleration, and the density of the fluid, the transition temperature T_λ at the midpoint of the resonator was determined[29] for each molar volume. The measured $T_{\lambda b} - T$ were then converted to $\theta_{vp} \equiv T_\lambda(\mathrm{SVP}) - T$ along the vapor pressure curve or to $t \equiv T_\lambda(V) - T$ along the isochores.

The pressure P_λ measured at the λ point and the corresponding temperature T_λ and molar volume V_λ are listed in Table II. Both V_λ and T_λ were determined from the measured P_λ and the equations given by Kierstead.[40] The directly measured T_λ's agree within 2 mK with the listed values. No independent measurements of V_λ were made.

Since the transition temperature is a function of the vertical position z in the resonator, the second-sound velocity is also a function of z, and the measured resonance frequency corresponds to some average velocity u_2. For large ϵ, i.e., far from T_λ, the velocity is no longer changing rapidly with temperature, and equating this average velocity to the second-sound velocity u_{2m} at the midpoint of the resonator is clearly a good approximation. As the transition is approached, this approximation will eventually fail, and the wave equation for the inhomogeneous medium will have to be solved for the resonance frequencies in order to obtain u_{2m}.[41] However, a perturbation calculation[42] in the small deviation

$$\delta(z) \equiv 1 - u_2^2(z)/u_{2m}^2$$

demonstrates that the measured average velocity at $\epsilon = 10^{-5}$ is equal to u_{2m} to within the precision of our data. We may therefore neglect the difference between u_2 and u_{2m} over the complete ϵ range of our measurements. We thus converted f/p directly to sound velocities, using Eq. (2) and the length l of the resonator. This length had been measured at room temperature to within 2.5×10^{-4} cm with a precision micrometer, and was corrected for thermal contraction.

The second-sound velocities along isochores

TABLE II. λ-point parameters at vapor pressure, and along the five experimental isochores.

P_λ (bar)	T_λ[a] (K)	V_λ[a] ($\mathrm{cm^3\ mole^{-1}}$)
SVP	2.172	27.38
7.27	2.096	25.32
12.13	2.036	24.41
18.06	1.956	23.53
24.10	1.865	22.80
29.09	1.782	22.28

[a]Determined from P_λ using the results of Ref. 40.

were corrected to sound velocities along isobars. This correction was made in two steps. First, the temperature distance from the transition line along isobars for each data point on the isochore was determined using[20]

$$\theta \equiv T_\lambda(P) - T = t + \Delta P\left(\frac{\partial T}{\partial P}\right)_\lambda, \tag{3}$$

with

$$\Delta P = P - P_\lambda = -\int_0^t \left(\frac{\partial P}{\partial T}\right)_v dt'.$$

Then the velocities, each along a slightly different isobar, were adjusted to the unique isobar which meets the λ line at the same point as the isochore, using

$$u_2(\theta, P_\lambda) = u_2(\theta, P) - \Delta P\left(\frac{\partial u_2}{\partial P}\right)_\theta.$$

This last correction is less than 1% of u_2 at $\theta \lesssim 10^{-2}$ K even at the highest pressures, and was first neglected. The derivative $(\partial u_2/\partial P)_\theta$ obtained from these intermediate results was then used to obtain the final isobaric data. The final results are listed in Table III. Although the SVP data are not strictly at constant pressure, the correction needed to bring them onto the isobar which has $P_\lambda = 0.0504$ bar is extremely small and was not applied.

As a test of our isochore-to-isobar conversion, one set of velocities was measured directly at 24.17 bar.[43] For these measurements the cell was joined via the capillary to a 3.3-liter reservoir which was immersed in a stirred water bath. The bath was regulated near room temperature to $\pm 3\times10^{-4}$ K.[20] Since the reservoir volume was very large compared to the cell volume, the experimental path followed by the liquid sample differed negligibly from an isobar. No correction was applied for the experimental path. The results differed by less than 1% from the smooth velocities calculated for this isobar from the isochore data.

The velocity along isobars within 20 mK of T_λ is shown graphically in Fig. 7 as a function of $T - T_\lambda(P)$ on linear scales. The velocity at each pressure tends to zero as the transition is approached, and at a given temperature distance from the transition decreases with increasing pressure. Along each isobar, the smallest velocity measurable with our transducers was approximately 50 cm/sec.

Figure 8 is a high-resolution plot of the velocity data. Previous results at SVP[13,44] indicated that the product $u_2^2\epsilon^{-0.772}$ is within the random errors of these earlier measurements independent of ϵ. We therefore plotted this parameter as a function of ϵ on logarithmic scales. The high resolution of this graph emphasizes any deviations from simple power-law behavior. Indeed, on each isobar our data

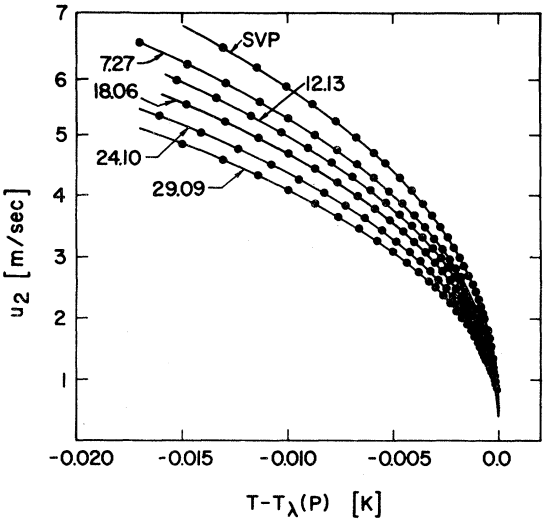

FIG. 7. Second-sound velocity at several constant pressures as a function of the temperature distance from the λ transition. The solid curves are smooth curves drawn through the data points. The number associated with each curve gives the pressure in bars.

reveal that $\log(u_2^2\epsilon^{-0.772})$ is neither a constant nor a linear function of $\log\epsilon$. This demonstrates that within our precision a function of the form

$$u_2^2(\epsilon, P) = g(P)\epsilon^{\Phi(P)}, \quad \epsilon \equiv 1 - T/T_\lambda(P) \tag{4}$$

is not adequate to represent the results. If Eq. (4) were adequate, then the data as presented in this figure would be along straight lines with slopes equal to the difference between Φ and 0.772.

We explicitly compare our data at vapor pressure with the results of Pearce, Lipa, and Buckingham.[44] These authors used a resonance technique, and generated and detected their second sound by means of a heater and thermometer, respectively. The solid horizontal line in Fig. 8 corresponds to the best power-law fit to their velocity data. There is fine agreement in magnitude, and the earlier results have the same *average* ϵ dependence as ours. However, the data by Pearce *et al.*[44] did not have the precision to reveal the departures from a simple power law. Although not indicated in Fig. 8, the present data are also consistent with the vapor-pressure results of Williams *et al.*[25] and Johnson and Crooks,[45] but differ systematically by a few percent from the measurements of Tyson and Douglass.[13] These latter results have an ϵ dependence, however, which appears consistent with that of our data; but of course they also do not reveal departures from pure power-law behavior.

The second-sound velocity under pressure has been measured recently by Terui and Ikushima[46] for $\epsilon \gtrsim 10^{-5}$. Their velocity measurements seem

TABLE III. Second-sound velocity u_2 and superfluid fraction ρ_s/ρ along isobars and near $T_\lambda(P)$.

SVP			7.27 bar			12.13 bar		
$1-T/T_\lambda(P)$	u_2 (cm/sec)	ρ_s/ρ	$1-T/T_\lambda(P)$	u_2 (cm/sec)	ρ_s/ρ	$1-T/T_\lambda(P)$	u_2 (cm/sec)	ρ_s/ρ
0.0415377	1347.78	0.291161	0.0091041	683.18	0.099753	0.0097319	657.10	0.099844
0.0366489	1288.65	0.268746	0.0079921	648.81	0.091233	0.0085334	623.29	0.091056
0.0323180	1231.12	0.247821	0.0070176	616.07	0.083418	0.0074756	591.12	0.083017
0.0284797	1175.19	0.228305	0.0061631	585.16	0.076316	0.0065589	560.97	0.075777
0.0250812	1120.45	0.209998	0.0053941	555.06	0.069662	0.0057412	531.65	0.069006
0.0220829	1067.92	0.193119	0.0047335	526.99	0.063686	0.0050366	504.35	0.062950
0.0194446	1017.38	0.177523	0.0041481	499.92	0.058139	0.0044185	478.67	0.0574.5
0.0150625	921.89	0.149730	0.0036411	474.48	0.053116	0.0038699	453.80	0.052376
0.0132471	877.15	0.137446	0.0032004	451.04	0.048668	0.0033894	430.55	0.047798
0.0116576	834.40	0.126147	0.0028095	428.21	0.044485	0.0029692	408.50	0.043624
0.0102462	793.25	0.115672	0.0024638	406.38	0.040635	0.0026038	387.67	0.039828
0.0089977	753.70	0.105974	0.0021648	385.97	0.037165	0.0022830	368.04	0.036390
0.0079116	716.54	0.097195	0.0018945	366.16	0.033923	0.0020041	349.42	0.033247
0.0068584	677.39	0.088294	0.0016543	347.15	0.030930	0.0017512	331.01	0.030255
0.0060043	642.83	0.080736	0.0014391	328.74	0.028144	0.0015286	313.60	0.027538
0.0052663	610.07	0.073824	0.0012631	311.54	0.025624	0.0013340	297.19	0.025079
0.0046131	579.10	0.067535	0.0011000	295.14	0.023326	0.0011651	281.59	0.022827
0.0040414	549.94	0.061825	0.0009656	280.55	0.021357	0.0010113	266.18	0.020693
0.0035348	521.57	0.056465	0.0008411	265.95	0.019462	0.0008867	252.78	0.018910
0.0030968	495.01	0.051624	0.0001711	144.30	0.006658	0.0007749	239.79	0.017245
0.0027091	469.64	0.047169	0.0001434	134.99	0.005917	0.0006782	227.39	0.015714
0.0024556	451.86	0.044145	0.0001216	126.81	0.005297	0.0005950	215.99	0.014362
0.0021514	428.89	0.040356	0.0001040	119.56	0.004772	0.0005126	203.30	0.012972
0.0018813	406.91	0.036863	0.0000897	113.09	0.004323	0.0004426	192.67	0.011758
0.0016449	386.14	0.033681	0.0000780	107.29	0.003937	0.0003980	184.77	0.010924
0.0014423	366.76	0.030816	0.0000682	102.06	0.003601	0.0003568	177.22	0.010153
0.0012563	347.58	0.028085	0.0000599	97.31	0.003308	0.0003168	169.04	0.009342
0.0011032	330.20	0.025694	0.0000530	92.99	0.003051	0.0002764	160.35	0.008513
0.0009691	314.02	0.023551	0.0000473	89.03	0.002823	0.0002419	152.43	0.007788
0.0008500	298.44	0.021559	0.0000423	85.40	0.002620	0.0002080	143.92	0.007038
0.0007486	284.06	0.019784	0.0000380	82.04	0.002438	0.0001855	137.85	0.006523
0.0006467	268.28	0.017907	0.0000342	78.95	0.002276	0.0001526	128.02	0.005724
0.0005624	254.29	0.016311	0.0000309	76.09	0.002131	0.0001274	119.46	0.005064
0.0004945	242.11	0.014971	0.0000281	73.41	0.001998	0.0001076	112.01	0.004517
0.0004269	228.53	0.013528	0.0000257	70.92	0.001877	0.0000917	105.42	0.004056
0.0003766	217.94	0.012450				0.0000789	99.56	0.003664
0.0003259	206.15	0.011292				0.0000683	94.31	0.003327
0.0003068	201.36	0.010833				0.0000595	89.60	0.003037
0.0002873	196.40	0.010369				0.0000520	85.34	0.002785
0.0002262	179.32	0.008834				0.0000460	81.46	0.002563
0.0001818	164.98	0.007624				0.0000408	77.91	0.002367
0.0001485	152.76	0.006652				0.0000362	74.67	0.002195
0.0001229	142.23	0.005861				0.0000324	71.68	0.002040
0.0001031	133.06	0.005206				0.0000292	68.92	0.001901
0.0000873	124.99	0.004657				0.0000263	66.36	0.001777
0.0000748	117.84	0.004192				0.0000239	64.00	0.001665
0.0000645	111.49	0.003798						
0.0000561	105.75	0.003455						
0.0000491	100.60	0.003160						
0.0000432	95.92	0.002902						
0.0000384	91.65	0.002673						
0.0000342	87.75	0.002472						
0.0000307	84.18	0.002294						
0.0000290	82.50	0.002213						
0.0000260	79.32	0.002062						

TABLE III. (*Continued*)

18.06 bar			24.10 bar			29.09 bar		
$1-T/T_\lambda(P)$	u_2 (cm/sec)	ρ_s/ρ	$1-T/T_\lambda(P)$	u_2 (cm/sec)	ρ_s/ρ	$1-T/T_\lambda(P)$	u_2 (cm/sec)	ρ_s/ρ
0.0098359	614.04	0.097643	0.0098366	564.01	0.095110	0.0095896	517.19	0.092805
0.0086254	581.94	0.088824	0.0086094	533.76	0.086177	0.0083792	488.31	0.083604
0.0075555	551.68	0.080845	0.0075410	505.38	0.078149	0.0073153	461.14	0.075343
0.0066126	522.66	0.073499	0.0065968	478.05	0.070749	0.0063915	435.46	0.067899
0.0057954	495.47	0.066898	0.0057645	452.18	0.064051	0.0055755	411.06	0.061159
0.0050660	469.11	0.060760	0.0050458	427.95	0.058053	0.0048573	387.92	0.055074
0.0044394	444.59	0.055282	0.0044172	405.16	0.052658	0.0042381	366.23	0.049644
0.0038890	421.48	0.050334	0.0038563	383.40	0.047735	0.0036973	346.00	0.044818
0.0034022	399.19	0.045752	0.0033751	362.86	0.043287	0.0032165	326.40	0.040362
0.0029775	378.31	0.041639	0.0029456	343.15	0.039205	0.0028027	308.23	0.036429
0.0026185	359.45	0.038074	0.0025753	324.86	0.035582	0.0024377	290.89	0.032850
0.0022947	340.80	0.034680	0.0022518	307.38	0.032265	0.0021201	274.58	0.029639
0.0017635	306.73	0.028843	0.0019773	291.72	0.029423	0.0018430	259.29	0.026768
0.0015405	290.51	0.026225	0.0017292	276.26	0.026730	0.0016750	249.43	0.024991
0.0013456	275.28	0.023870	0.0015143	261.82	0.024318	0.0014655	235.97	0.022646
0.0011744	260.87	0.021728	0.0013213	247.79	0.022070	0.0012817	223.31	0.020538
0.0010275	247.26	0.019782	0.0011506	234.36	0.020009	0.0011189	211.27	0.018619
0.0008934	233.85	0.017942	0.0010005	221.54	0.018124	0.0009732	199.65	0.016848
0.0007836	222.04	0.016386	0.0008745	209.92	0.016487	0.0008477	188.70	0.015250
0.0006886	211.04	0.014991	0.0007587	198.29	0.014914	0.0007391	178.50	0.013824
0.0006041	200.24	0.013670	0.0006635	188.02	0.013584	0.0006417	168.66	0.012509
0.0005314	190.46	0.012522	0.0005795	178.21	0.012363	0.0005618	159.83	0.011375
0.0004583	179.76	0.011314	0.0005069	168.98	0.011260	0.0004914	151.55	0.010358
0.0003998	170.38	0.010298	0.0004451	160.52	0.010287	0.0004305	143.61	0.009417
0.0003522	162.15	0.009438	0.0003831	151.36	0.009277	0.0003780	136.36	0.008595
0.0003052	153.31	0.008552	0.0003314	142.98	0.008392	0.0003345	129.92	0.007892
0.0002694	146.15	0.007863	0.0002896	135.62	0.007646	0.0002910	122.93	0.007158
0.0002343	138.40	0.007141	0.0002494	127.62	0.006865	0.0002571	117.03	0.006562
0.0002709	146.47	0.007893	0.0002191	121.35	0.006280	0.0002230	110.63	0.005941
0.0002316	137.86	0.007093	0.0001886	114.35	0.005654	0.0001977	105.51	0.005464
0.0001958	129.18	0.006325	0.0002611	129.74	0.007065	0.0001724	99.99	0.004968
0.0001722	122.71	0.005773	0.0002323	123.88	0.006511	0.0001513	95.07	0.004544
0.0001481	115.76	0.005206	0.0002016	117.25	0.005908	0.0001306	89.77	0.004105
0.0001312	110.74	0.004816	0.0001759	111.07	0.005368	0.0001153	85.50	0.003764
0.0001139	104.90	0.004376	0.0001558	106.07	0.004950	0.0001009	81.22	0.003437
0.0001080	102.79	0.004220	0.0001359	100.60	0.004506	0.0000888	77.34	0.003151
0.0000941	97.51	0.003843	0.0001213	96.32	0.004172	0.0000787	73.82	0.002901
0.0000825	92.76	0.003517	0.0001136	93.98	0.003995	0.0000700	70.63	0.002682
0.0000728	88.44	0.003231	0.0000979	88.76	0.003611	0.0000626	67.69	0.002487
0.0000646	84.50	0.002979	0.0000850	84.09	0.003280	0.0000561	64.97	0.002312
0.0000576	80.91	0.002757	0.0000744	79.89	0.002994	0.0000507	62.47	0.002156
0.0000516	77.61	0.002560	0.0000655	76.08	0.002744	0.0000458	60.15	0.002016
0.0000464	74.57	0.002384	0.0000578	72.62	0.002527	0.0000416	58.02	0.001890
0.0000418	71.76	0.002226	0.0000516	69.46	0.002334	0.0000379	56.00	0.001774
0.0000397	70.42	0.002153	0.0000461	66.56	0.002163	0.0000346	54.14	0.001670
0.0000360	67.90	0.002017	0.0000413	63.91	0.002012	0.0000316	52.40	0.001576
0.0000327	65.56	0.001895	0.0000372	61.45	0.001876	0.0000291	50.76	0.001489
0.0000300	63.39	0.001783	0.0000338	59.17	0.001753	0.0000267	49.22	0.001409
0.0000274	61.33	0.001681	0.0000306	57.05	0.001642	0.0000247	47.77	0.001336
0.0000252	59.41	0.001588	0.0000280	55.10	0.001543	0.0000228	46.41	0.001269
0.0000232	57.61	0.001503	0.0000255	53.26	0.001452			

to be as precise as ours, but apparently their values of $T_\lambda - T$ have slightly larger errors.[47] Their results appear to be consistent with the present data. The second-sound velocity under pressure has also been measured recently by Brillouin light scattering. These measurements typically have errors of the order of 1%. The data of both Winterling *et al.*[48] for $\epsilon \gtrsim 10^{-4}$ at 25.3

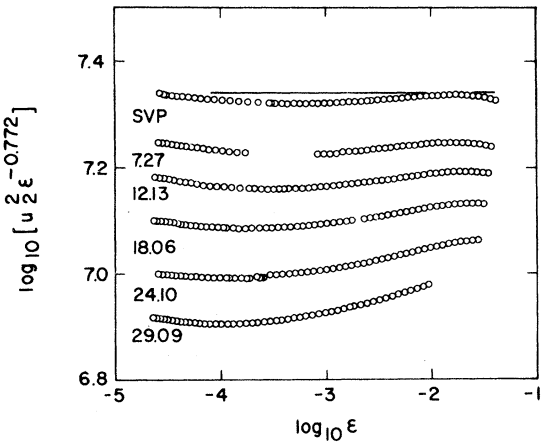

FIG. 8. High-resolution plot of the second-sound velocity u_2 (in cm/sec) along isobars. The numbers give the pressure in bars. The solid line is the best fit to the results of Pearce, Lipa, and Buckingham (Ref. 44). The 29.09-bar data at large ϵ extend to the melting curve.

bar and of Vinen *et al.*[49] for $\epsilon \gtrsim 2\times10^{-4}$ at 20 bar agree with the present measurements.

In order to provide a closed-form expression for the velocity which is useful in many thermohydrodynamic calculations, we have fitted all of the data with $\epsilon < 10^{-2}$ to the expression

$$u_2 = h(P)\epsilon^{1/3}[1 + b(P)\epsilon^{1/6}], \quad \epsilon \equiv 1 - T/T_\lambda(P) \qquad (5)$$

with

$$h(P) = h_0 + h_1 P$$

and

$$b(P) = b_0 + b_1 P + b_2 P^2 .$$

In Fig. 9 the percent deviations of the data from this fit are plotted. If we ignore the larger deviations of the data with $\epsilon \lesssim 6\times10^{-5}$ at 29.09 bar, Eq. (5) is adequate to describe the data within $\frac{1}{2}\%$ over the complete ϵ range of the fit. The larger deviations at the highest pressure for the smallest ϵ

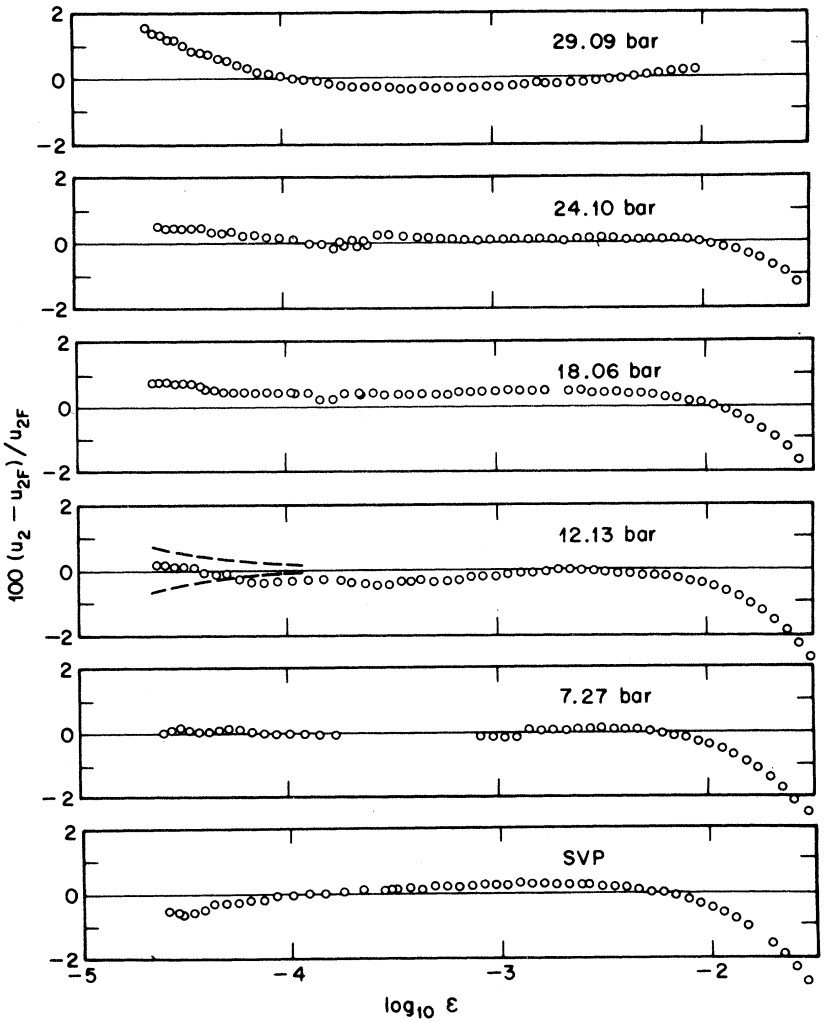

FIG. 9. Deviations of the measured u_2 from the velocity u_{2F} which is given by Eq. (5). The dashed curves for 12.13 bar indicate deviations corresponding to errors in T_λ of $\pm 1\,\mu$K.

may be in part due to a larger error in the measured $T_\lambda(P)$ than our estimated ± 1 μK. The sensitivity of the deviations in Fig. 9 to errors in T_λ is demonstrated by the dashed curves drawn in the 12.13-bar plot. These curves correspond to the change in the deviations which was obtained when T_λ (12.13) was changed by ± 1 μK.

B. Superfluid Density

The superfluid density ρ_s near T_λ can be determined from the present measurements of u_2, other already available[18–20] thermodynamic information, and a relation based on linear two-fluid hydrodynamics.[50] To second order in u_{20}/u_{10}, u_2 is related to ρ_s by

$$u_2^2 = u_{20}^2[1 - (\gamma - 1)u_{20}^2/u_{10}^2], \tag{6}$$

where

$$u_{20}^2 \equiv S^2 T \rho_s / \rho_n C_p,$$

$$u_{10}^2 \equiv \left(\frac{\partial P}{\partial \rho}\right)_S,$$

$$\gamma \equiv C_p / C_v.$$

Here C_p and C_v are the heat capacities at constant pressure and at constant volume, respectively, and S is the entropy. Although the specific-heat ratio γ may diverge as the λ transition is approached, $\gamma - 1$ remains less than 1 for $\epsilon > 10^{-5}$ even at the highest pressure.[20] The small expansion parameter in Eq. (6) is u_{20}^2/u_{10}^2, which vanishes at T_λ approximately as $\epsilon^{2/3}$ and is much less than unity at all temperatures and pressures. Over the complete range of our data u_{20} differs from u_2 by less than our resolution; this difference has therefore been neglected.

The entropy $S(P, \epsilon)$ was obtained from the calorimetric entropy $S_{\lambda 0} = 6.24$ J mole^{-1} K^{-1} at vapor pressure and T_λ[51,52] by first integrating the relation[20]

$$\left(\frac{\partial S}{\partial T}\right)_\lambda = 1.97 + 0.0938(1 - T_\lambda/2.260)^{-1.380} \text{ J mole}^{-1}\text{ K}^{-2}$$

along the λ line to yield $S(P, 0) - S_{\lambda 0}$, and by then integrating

$$C_p/T = (1/T)(-A \ln\epsilon + B + D\epsilon \ln\epsilon + E\epsilon) \tag{7}$$

along the isobar. To order ϵ^2, one obtains

$$S(P, \epsilon) - S(P, 0) = A\epsilon \ln\epsilon + \tfrac{1}{2}(A - D)\epsilon^2 \ln\epsilon - (A + B)\epsilon - \tfrac{1}{4}(A - D + 2B + 2E)\epsilon^2 . \tag{8}$$

The parameters in Eqs. (7) and (8) are given by[20]

$$\begin{aligned} A &= 5.102 - 0.05652P + 9.643\times10^{-4}P^2, \\ B &= 15.57 - 0.3601P + 4.505\times10^{-3}P^2, \\ D &= +14.5 - 6.119P, \\ E &= -69.0 - 19.08P, \end{aligned} \tag{9}$$

with P in bar and C_p in J mole^{-1} K^{-1}. The resulting calculated values of ρ_s/ρ are listed in Table III. The data extend out to $\epsilon = 10^{-1}$ at SVP and out to $\epsilon = 10^{-2}$ at $P >$ SVP. These limits were imposed by the range of validity[20] of Eqs. (7) and (9). A few values of ρ_s/ρ were calculated at larger ϵ using other appropriate thermodynamic information[51,53–55] in numerical form. These values will be indicated in a following figure.

The results for ρ_s/ρ along three isobars are shown graphically as a function of ϵ on logarithmic scales in Fig. 10. It can be seen that the three sets of data are not quite parallel to each other. If the simple power law

$$\rho_s/\rho = k(P)\epsilon^\zeta \tag{10}$$

is used to describe the results, then the slopes of straight lines through the data are equal to ζ. Thus, the use of Eq. (10) with the measurements will result in values of ζ which are slightly dependent upon pressure. This observation was made also by Terui and Ikushima[46] on the basis of their own measurements of u_2. However, a closer examination of Fig. 10 reveals some slight curvature in the data at the higher pressures even for small ϵ. This curvature indicates that Eq. (10) is not adequate to describe the measurements, and that a fit of the data to Eq. (10) will not yield an exponent ζ characteristic of the asymptotic behavior of ρ_s.

In order to facilitate comparison with the results of Terui and Ikushima, we fitted the measurements at each pressure with $\epsilon < 10^{-2.3}$ to Eq. (10) although we know that Eq. (10) is not of the correct functional form. The results are shown in Fig. 11. They reveal a pressure dependence of the apparent exponent which is in over-all agreement with the results of Terui and Ikushima.[46] The general trend

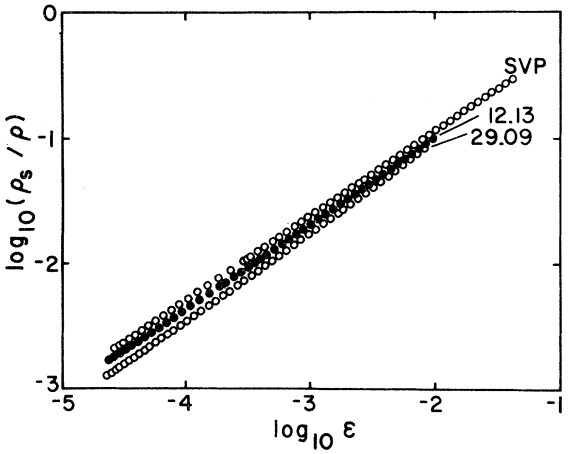

FIG. 10. Superfluid fraction ρ_s/ρ derived from measurements of u_2 vs ϵ. The numbers give the pressure in bars.

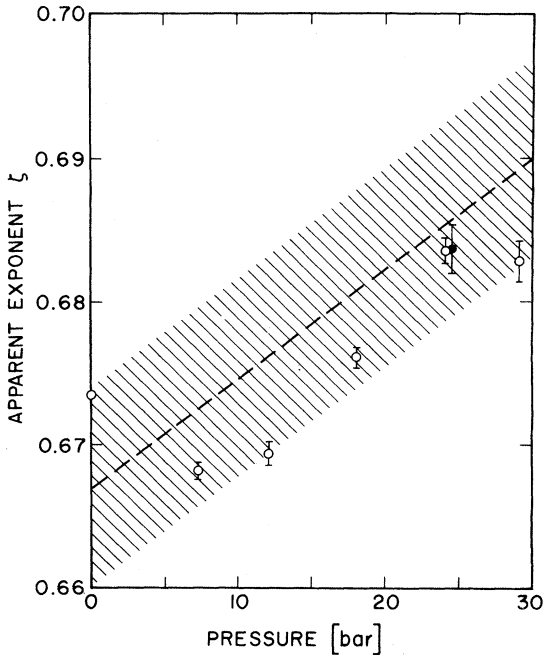

FIG. 11. Apparent critical exponent for ρ_s/ρ resulting from a fit of the data with $\epsilon < 10^{-2.3}$ to Eq. (10). All results pertain to isobars, but the open circles are based on values of u_2 derived from measurements along isochores, whereas the solid circle is based on the measurements directly along an isobar.

and approximate range of uncertainty of their exponent is indicated by the shaded area in the figure.

At SVP, we can compare our ρ_s/ρ with several other results which are based upon a variety of experiments and predictions of two-fluid hydrodynamics.[11] For this comparison, we will again use Eq. (10). Our data yield an effective exponent $\zeta_{\text{eff}}^{\text{SVP}} = 0.674 \pm 0.001$, where the indicated error is based upon the (presumably inapplicable) assumption that Eq. (10) is the correct functional form. This result can be compared with measurements by Tyson and Douglass.[14] These authors used the Andronikashvili method,[56] which involves measuring the period of a torsional pendulum consisting of many closely spaced disks oriented perpendicular to the pendulum axis. The normal fluid trapped between the disks contributes to the moment of inertia of the pendulum, and thus affects the period. They obtained $\zeta_{\text{eff}}^{\text{SVP}} = 0.666 \pm 0.006$, which is in satisfactory agreement with our result. Clow and Reppy[12] measured the angular momentum of a persistent superfluid current by means of a gyroscopic technique. This work yielded $\zeta_{\text{eff}}^{\text{SVP}} = 0.67 \pm 0.03$, again in agreement with the other results. Finally, Kriss and Rudnick[16] measured the velocity of fourth sound u_4 in He II contained in a porous medium where the viscous drag on the normal fluid is sufficiently large to assure that the normal fluid velocity is zero. For this case, two-fluid hydrodynamics also yields a relation between ρ_s/ρ, u_4, and the thermodynamic parameters. Kriss and Rudnick obtain $\zeta_{\text{eff}}^{\text{SVP}} = 0.665 \pm 0.005$. Although this value of ζ_{eff} appears appreciably lower than ours, the difference is only 1.5 times the sum of the quoted errors and not necessarily significant. We conclude that the four sets of measurements yield the same ρ_s/ρ within the rather small experimental errors, and regard this as a detailed confirmation of the validity of the hydrodynamics even near T_λ where the parameters in the theory are singular.

Since we found that ρ_s/ρ is at least approximately proportional to $\epsilon^{2/3}$, we present a high-resolution graph of ρ_s/ρ in Fig. 12 by plotting the product $(\rho_s/\rho)\cdot\epsilon^{-2/3}$ vs ϵ on logarithmic scales. This figure shows more clearly the curvature which was first revealed in Fig. 10. As in Fig. 10, if ρ_s/ρ is accurately described by Eq. (10), then the data should fall on straight lines, but now with slopes equal to $\zeta - \frac{2}{3}$. At the higher pressures the curvature extends to the smallest values of ϵ, and it is evident that a more complicated function than Eq. (10) is needed to represent the results over any reasonable range of ϵ. Before analyzing our results in more detail, however, we shall use Fig. 12 for a comparison with additional measurements by others under pressure and at larger ϵ.

The solid horizontal line in Fig. 12 at SVP corresponds to $\zeta = \frac{2}{3}$, and represents the best fit to the data at SVP of Tyson[14] which we already discussed. For $P \lesssim 20$ bar and at fairly large ϵ, our data are compared with the results of Romer and

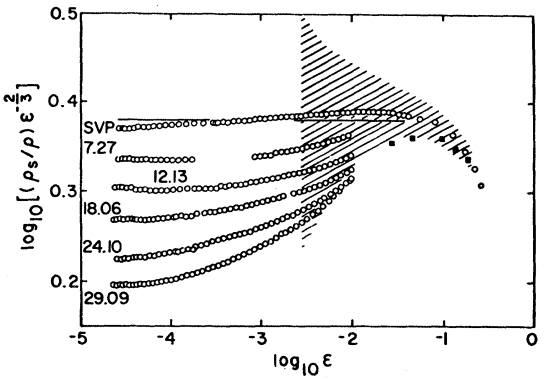

FIG. 12. High-resolution plot of the superfluid fraction ρ_s/ρ along isobars derived from measurements of u_2. The numbers give the pressure in bars. The solid squares correspond to u_2 at 25.3 bar measured by Peshkov and Zinov'eva (Ref. 38). The solid line represents values of ρ_s/ρ at vapor pressure measured by Tyson (Ref. 14). The shaded area corresponds to the range of values of $(\rho_s/\rho)\epsilon^{-2/3}$ under pressure permitted by the results of Romer and Duffy (Ref. 15).

Duffy[15] which were obtained by the Andronikashvili pendulum technique. These results fall on a universal curve that nearly coincides with the present measurements at vapor pressure. However, the permitted systematic error in the Romer and Duffy results increases rapidly with decreasing ϵ. The range of permitted values of $(\rho_s/\rho)\epsilon^{-2/3}$ shown by the shaded area in the figure is consistent with our measurements at all pressures. Values of ρ_s/ρ for $\epsilon > 10^{-2}$ were computed also from the u_2 measurements by Peshkov and Zinov'eva[38] at 25.3 bar and are shown in Fig. 12 as solid squares. They are consistent with the trend of our results at similar pressures and smaller ϵ. We also calculated ρ_s/ρ for $\epsilon > 10^{-2}$ from our u_2 at 20.3 bar. These results, although not shown in Fig. 12, fall very close to the solid squares.

Although it is clear that singular correction terms to the simple power law Eq. (10) are needed, it is not possible to determine from the measurements the functional form of the corrections to the asymptotic behavior of ρ_s/ρ. It was thus assumed that the departures of ρ_s/ρ from Eq. (10) can themselves be described by a power law with an exponent which is larger than ζ. Explicitly, we have compared the data with the function

$$\rho_s/\rho = k(P)\epsilon^{\zeta}[1 + a(P)\epsilon^{y}], \quad y > 0. \tag{11}$$

In fitting our results to this relation, each of the data points was weighted. In our measurements, the error in ϵ is far more important than the error in ρ_s/ρ, and therefore we used a weight $W = [\delta(\rho_s/\rho)]^{-2}$, where $\delta(\rho_s/\rho)$ is the estimated uncertainty in ρ_s/ρ which corresponds to our uncertainty in ϵ if we make the approximation $\rho_s/\rho \propto \epsilon^{2/3}$. The weighting function was thus given by $W = \epsilon^{2/3}(\delta\epsilon)^{-2}$. For $\delta\epsilon$, we used the larger of $10^{-3}\epsilon$ and 2×10^{-7}. An estimate of systematic errors was made for each least-squares fit by changing ϵ by 1×10^{-6} and refitting the data. In Figs. 13–16 possible systematic errors determined in this manner are included in the error bars.

The data with $\epsilon < 10^{-2.4}$ at each pressure were fitted to Eq. (11) for several fixed values of y, and the resulting best values of ζ for each y are plotted in Fig. 13. The estimated uncertainties of ζ are now much larger than the ± 0.001 which we quoted above for SVP. This is attributable to the larger number of parameters in Eq. (11) as compared to Eq. (10), and is a consequence of the increased statistical correlation between these parameters. Within these larger uncertainties, ζ at SVP is nearly independent of y. As the pressure increases, however, the y dependence of ζ also increases and becomes strongest at the highest pressures. If both ζ and y in Eq. (11) are to be independent of pressure, then the SVP results in Fig. 13 would indicate $\zeta \approx 0.67$. As a guide for comparison a reference line with ζ near this value is shown as a dashed line through the results for each isobar. The intersection of this reference line with $\zeta(y)$ at 29.09 bar would then imply $y \approx 0.5$. At 24.10

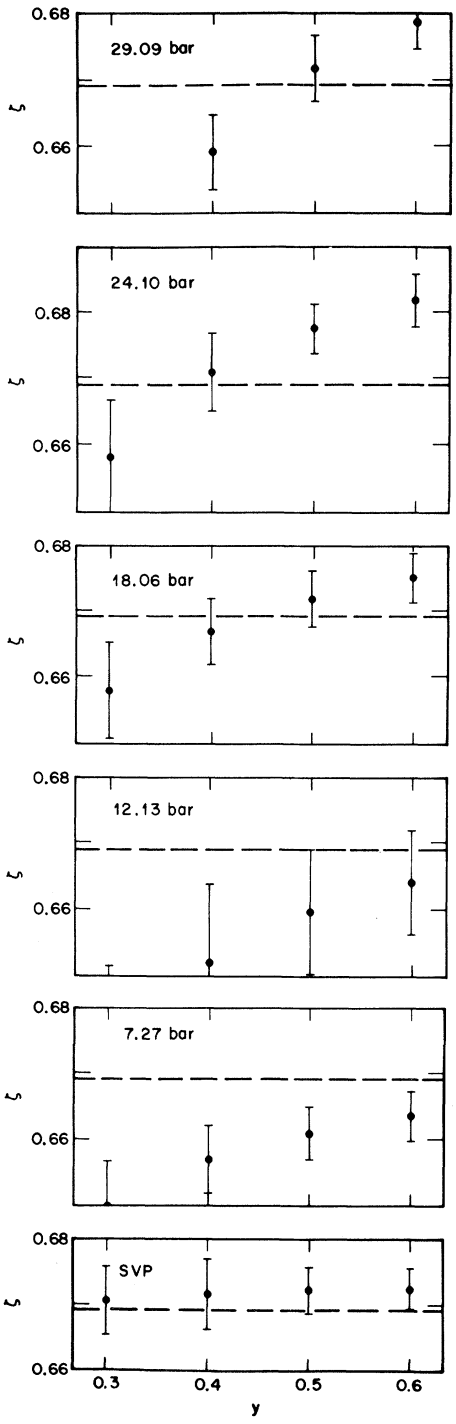

FIG. 13. Superfluid-fraction exponent ζ determined by fitting the ρ_s/ρ data with $\epsilon < 10^{-2.4}$ to Eq. (11) with fixed values of y.

bar and $y = 0.5$, ζ is slightly larger than 0.67 while at 7.27 bar and $y = 0.5$, ζ is less than 0.67. These deviations cannot be consider as significant since they may correspond to a slight underestimate of systematic errors. The results thus are consistent with both ζ and y independent of pressure with[57]

$$0.66 \lesssim \zeta \lesssim 0.68$$

and (12)

$$0.4 \lesssim y \lesssim 0.6 .$$

As a further test of the appropriateness of Eq. (11) with $y = 0.5$ we have taken the 24.10-bar data and computed the best parameters ζ, k, and a, considering only data with $\epsilon < \epsilon_{max}$. These parameters are plotted versus ϵ_{max} in Fig. 14, and clearly indicate that ζ, k, and a do not depend on the range of data included in the fit. Therefore, at least for this particular isobar, the data are well represented by Eq. (11).

The pressure dependences of ζ, k, and a, which result from the fits to Eq. (11) with $y = 0.5$ for data with $\epsilon < 10^{-2.4}$, are shown in Fig. 15. The deviations from each of the three dashed reference curves, which are evident for some of the isobars, are all related to each other and reflect the correlations between the three parameters. Forcing $\zeta \approx 0.67$ at 7.27 bar, for example, causes k to increase and a to decrease. We performed a combined least-squares fit of the data at all pressures with $\epsilon < 10^{-2.4}$ to Eq. (11). In this fit, we used $y = 0.5$ and forced ζ to be independent of pressure. With these constraints, it was possible to represent k and a by the simple polynominals

$$k = k_0 + k_1 P ,$$

$$a = a_0 + a_1 P + a_2 P^2 .$$

We find as a good closed-form expression for the superfluid fraction

$$\rho_s/\rho = k(P)\epsilon^{0.6692}[1 + a(P)\epsilon^{0.5}] , \quad (13)$$

with

$$k(P) = 2.396 - 0.02883P ,$$

$$a(P) = 0.6514 - 0.04548P + 0.005265P^2 .$$

The dashed reference curves in Figs. 13 and 15 were determined using this expression. The devia-

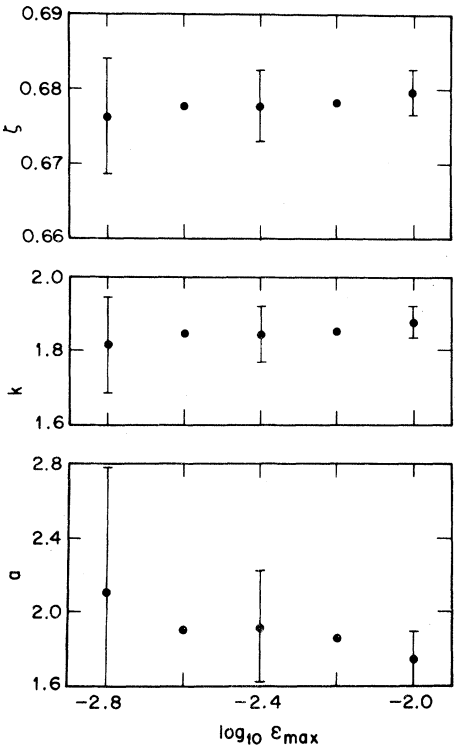

FIG. 14. Parameters ζ, k, and a obtained by fitting the ρ_s/ρ data at 24.10 bar with $\epsilon < \epsilon_{max}$ to Eq. (11) with $y = 0.5$, as a function of ϵ_{max}.

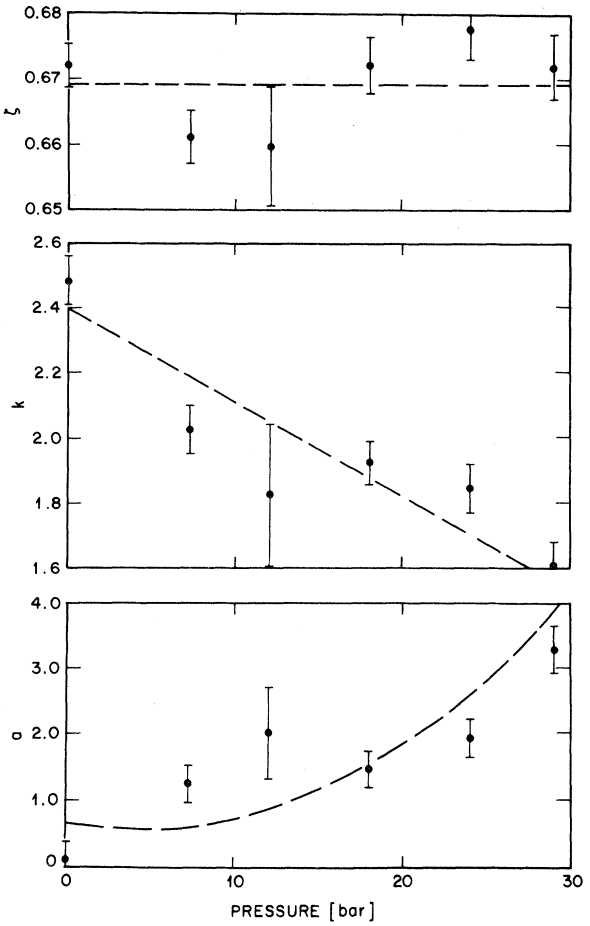

FIG. 15. Parameters ζ, k, and a obtained by fitting the ρ_s/ρ data along each isobar with $\epsilon < 10^{-2.4}$ to Eq. (11) with $y = 0.5$, as a function of pressure.

tions of the data in percent from Eq. (13) are shown in Fig. 16.

IV. COMPARISON WITH THEORY

According to the Josephson scaling law,[5] the exponent ζ of ρ_s/ρ is related to the exponent β of the order parameter by

$$\zeta = 2\beta - \eta\nu' . \tag{14}$$

Here ν' is the exponent of the coherence length ξ for fluctuations in the order parameter below T_λ, and η describes the deviations of the correlation function from Ornstein–Zernike behavior.[1] Near the superfluid transition, β, η, and ν' are not readily accessible to direct measurement; but with the aid of other scaling laws due to Widom[2] and Kadanoff,[3] Eq. (14) can be transformed into[5]

$$\zeta = \tfrac{1}{3}(2 - \alpha'), \tag{15}$$

where α' describes the singularity in the heat capacity at constant pressure as T_λ is approached from below. Equation (15) can be subjected to an experimental test. The result [Eq. (12)] that independent of pressure

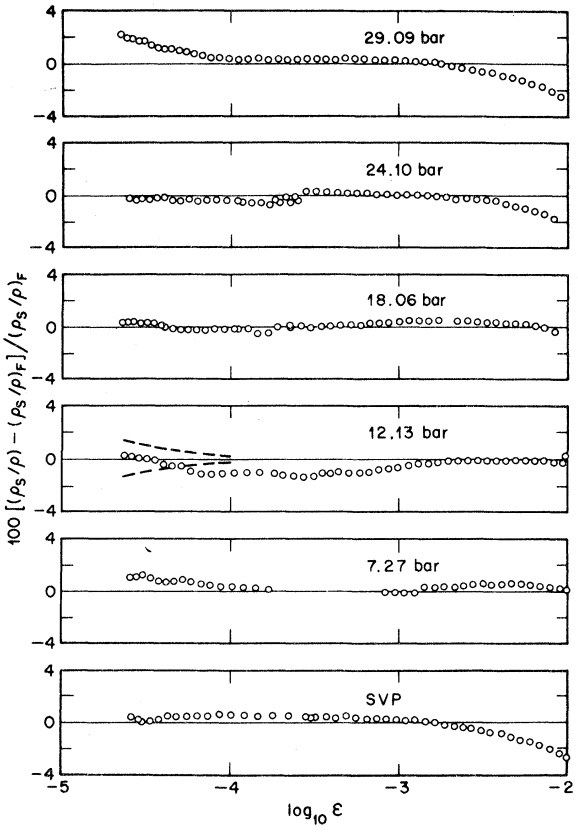

FIG. 16. Deviations of the ρ_s/ρ data from the values $(\rho_s/\rho)_F$ calculated using Eq. (13). The dashed curves indicate deviations corresponding to errors in T_λ of $\pm 1\,\mu$K.

$$\zeta = 0.67 \pm 0.01$$

implies with Eq. (15) that

$$\alpha' = -0.01 \pm 0.03 . \tag{16}$$

This is consistent with the experimental specific-heat results[18–20] which also yield[20] Eq. (16) for α' independent of pressure. This value of α' was obtained in an analysis of the data which considered the possibility that singular higher-order terms contribute appreciably to C_p in both the low- and high-temperature phases. The fact that for both ζ and α' the experimental data permit an interpretation in which neither exponent is pressure dependent is consistent with theoretical expectations based on universality arguments.[6] According to universality one expects the critical-point behavior to depend only on the spatial dimensionality of the system and on the number of degrees of freedom in the order parameter. For the case of the λ transition in helium, universality then implies that the critical-point exponents should not be affected by changes in an inert variable such as the pressure, which does not alter the basic character of the transition.

Recently, explicit calculations of exponents by an expansion in the dimensionality d (i.e., $d=3$ in our case) have become possible.[7,8] These expansions support the concept of universality, and together with scaling[2,3] yield to second order in $(4-d)$ the value $\zeta = 0.673$ for a system like the superfluid transition with two degrees of freedom in the order parameter. In addition, a calculation of the correction-term exponent to first order in $(4-d)$ has been performed by Wegner,[9] and gives $y \approx 0.5$ and roughly independent of the type of transition. Both of these values are consistent with the present experimental results.

On the basis of the high precision and temperature resolution of the data we had hoped to provide a very accurate value of the exponent ζ. But because ρ_s/ρ *cannot* be represented by a simple power law in ϵ like Eq. (11) with $a(P)\equiv 0$, the experimental uncertainty in all parameters is still sizable. However, even with the large number of parameters in Eq. (11), it should be possible to reduce the uncertainty of ζ considerably below our present value by measurement of ρ_s with more accurate determinations of T_λ. The same is not true for the specific heat, where the uncertainty in T_λ is already nearly an order of magnitude smaller. For C_p, the uncertainty in the exponent is larger for data with the same general precision because the additive constant, which is always present for this variable, introduces an additional degree of freedom into the fit. A significant improvement in the C_p measurements does not at present seem experimentally feasible. On the other hand, improve-

ments in the second-sound velocity experiment seem straightforward. Measurements with a more accurate value of T_λ should be capable of providing exponents ζ and y which would provide a more stringent test of the concept of universality. Because of the greater latitude in α', however, it is not likely that the scaling law Eq. (15) can be tested readily with greater precision.

V. SUMMARY

Using superleak condenser transducers in a thermally isolated resonance cavity, the velocity of second sound was measured at temperatures very near the superfluid transition in pure ^{4}He, under saturated vapor pressure and along five isochores. The isochoric data were converted to velocities along isobars. Where comparison was possible, the present second-sound velocities were consistent with less precise previous measurements. Via a result of two-fluid hydrodynamics the second-sound velocities, in conjunction with other appropriate thermodynamic data, were used to determine the superfluid fraction ρ_s/ρ. These results were again consistent with the less precise values determined by others using different methods. The precision of the present ρ_s/ρ data clearly indicated that a simple power law was not an adequate representation of the data over any reasonable range of ϵ. When a singular correction term which contributed appreciably even for small ϵ [see Eq. (11)] was included in the analysis, the data were seen to be consistent with a leading exponent $0.66 < \zeta < 0.68$ and a correction exponent $0.4 < y < 0.6$, independent of the pressure. The lack of a pressure dependence of ζ and y is in agreement with universality. The exponent ζ is in agreement with the value determined using the experimental specific-heat exponent α' and the scaling relation $\zeta = \frac{1}{3}(2 - \alpha')$. Both ζ and y are consistent with recent explicit theoretical calculations.

ACKNOWLEDGMENTS

We are grateful to M. Barmatz, P. C. Hohenberg, and J. B. Lastovka for helpful discussions and advice concerning various aspects of this work.

[1]See, for example, H. E. Stanley, *Introduction to Phase Transitions and Critical Phenomena* (Oxford U.P., New York, 1971).

[2]B. Widom, J. Chem. Phys. 43, 3892 (1965); J. Chem. Phys. 43, 3898 (1965).

[3]L. P. Kadanoff, Physics 2, 263 (1966).

[4]R. B. Griffiths, Phys. Rev. 158, 176 (1967).

[5]B. D. Josephson, Phys. Letters 21, 608 (1966).

[6]See, for instance, L. P. Kadanoff, in *Proceedings of the International School of Physics "Enrico Fermi", Course LI*, edited by M. S. Green (Academic, New York, 1971); R. B. Griffiths, Phys. Rev. Letters 24, 1479 (1970).

[7]K. G. Wilson and M. E. Fisher, Phys. Rev. Letters 28, 240 (1972); K. G. Wilson, Phys. Rev. Letters 28, 548 (1972).

[8]E. Brézin, D. J. Wallace, and K. G. Wilson, Phys. Rev. Letters 29, 591 (1972); Phys. Rev. B 7, 232 (1973).

[9]F. J. Wegner, Phys. Rev. B 5, 4529 (1972).

[10]See, for instance, Ref. 5.

[11]I. M. Khalatnikov, *Introduction to the Theory of Superfluidity* (Benjamin, New York, 1965).

[12]J. R. Clow and J. D. Reppy, Phys. Rev. Letters 16, 887 (1966); Phys. Rev. A 5, 424 (1972).

[13]J. A. Tyson and D. H. Douglass, Phys. Rev. Letters 21, 1308 (1968).

[14]J. A. Tyson and D. H. Douglass, Jr., Phys. Rev. Letters 17, 472 (1966); J. A. Tyson, Phys. Rev. 166, 166 (1968).

[15]R. H. Romer and R. J. Duffy, Phys. Rev. 186, 255 (1969).

[16]M. Kriss and I. Rudnick, J. Low Temp. Phys. 3, 339 (1970).

[17]See, for instance, M. E. Fisher, Rep. Prog. Phys. 30, 615 (1967).

[18]G. Ahlers, Phys. Rev. Letters 23, 464 (1969); Phys. Rev. A 3, 696 (1971).

[19]G. Ahlers, in *Proceedings of the Twelfth International Conference on Low Temperature Physics*, edited by E. Kanda (Academic of Japan, Tokyo, 1971), p. 21.

[20]G. Ahlers, Phys. Rev. A (to be published).

[21]B. I. Halperin and P. C. Hohenberg, Phys. Rev. Letters 19, 700 (1967); Phys. Rev. 177, 952 (1969).

[22]D. S. Greywall and G. Ahlers, Phys. Rev. Letters 28, 1251 (1972).

[23]D. S. Greywall and G. Ahlers, in Proceedings of the Thirteenth International Conference on Low Temperature Physics, Boulder, Colo., 1972 (unpublished).

[24]P. M. Morse, *Vibration and Sound*, 2nd ed. (McGraw-Hill, New York, 1948), p. 397.

[25]R. Williams, S. E. A. Beaver, J. C. Fraser, R. S. Kagiwada, and I. Rudnick, Phys. Letters 29A, 279 (1969).

[26]R. A. Sherlock and D. O. Edwards, Rev. Sci. Instr. 41, 1603 (1970).

[27]General Electric Co., Pleasanton, Calif.

[28]Krylon, Inc., Norristown, Pa.

[29]G. Ahlers, Phys. Rev. 171, 275 (1968).

[30]H. van Dijk, M. Durieux, J. R. Clement, and J. K. Logan, Natl. Bur. Std. (U.S.) Monograph No. 10 (U.S. GPO, Washington, D.C., 1960).

[31]M. Barmatz and I. Rudnick, Phys. Rev. 170, 224 (1968).

[32]General Radio wave analyzer, Type 1900-A.

[33]Heath multispeed chart drive.

[34]Using an unbiased drive transducer reduces the amount of "cross talk" detected by the analyzer. Since a signal of frequency $f/2$ is delivered to the resonator, the direct "pickup" is due only to the small second-harmonic distortion of frequency f.

[35]Wavetek function generator, Model 116.

[36]Princeton Applied Research preamplifier, Model 113.

[37]For a description of the sample gas and pressure measuring system, see Refs. 18 and 20.

[38]V. P. Peshkov and K. N. Zinov'eva, Zh. Eksp. Teor.

Fiz. 18, 438 (1948).
[39]R. D. Mauer and M. A. Herlin, Phys. Rev. 81, 444 (1951).
[40]H. A. Kierstead, Phys. Rev. 162, 153 (1967).
[41]P. C. Hohenberg and M. Barmatz, Phys. Rev. B 6, 289 (1972).
[42]P. M. Morse, *Vibration and Sound*, 2nd ed. (McGraw-Hill, New York, 1948), p. 122.
[43]It is apparent that all our measurements could have been made directly along isobars. However, the temperature stability of our reference pressure bath of $\pm 3\times10^{-4}$ °C corresponds to ± 1 ppm in the pressure. (See also Sec. II A1 of Ref. 20.) Near the melting pressure, this corresponds to $\pm 3\times10^{-5}$ bars, which in turn corresponds to ± 0.5 μK for the stability of T_λ. In principle, it is possible to hold the density on isochores sufficiently constant to reduce variations in T_λ by an order of magnitude below this level, although in the present work such high stability was not achieved (see Sec. II D).
[44]C. J. Pearce, J. A. Lipa, and M. S. Buckingham, Phys. Rev. Letters 20, 1471 (1968).
[45]D. L. Johnson and M. J. Crooks, Phys. Rev. 185, 253 (1969).
[46]G. Terui and A. Ikushima, Phys. Letters 39A, 161 (1972); A. Ikushima and G. Terui, J. Low Temp. Phys. 10, 397 (1973).
[47]A. Ikushima (private communication).
[48]G. Winterling, F. S. Holmes, and T. J. Greytak, in Proceedings of the Thirteenth International Conference on Temperature Physics, Boulder, Colo., 1972 (unpublished); Phys. Rev. Letters 30, 427 (1973).
[49]W. F. Vinen, C. J. Palin, and J. M. Vaughan, in Proceedings of the Thirteenth International Conference on Low Temperature Physics, Boulder, Colo., 1972 (unpublished).
[50]I. M. Khalatnikov, *Introduction to the Theory of Superfluidity* (Benjamin, New York, 1965), Chap. 10.
[51]R. W. Hill and O. V. Lounasmaa, Phil. Mag. 2, 143 (1957).
[52]C. G. Waterfield, J. K. Hoffer, and N. E. Phillips (unpublished).
[53]D. L. Elwell and H. Meyer, Phys. Rev. 164, 245 (1967).
[54]H. C. Kramers, J. D. Wasscher, and C. J. Gorter, Physics 18, 329 (1952).
[55]O. V. Lounasmaa, Cryogenics 1, 212 (1961).
[56]See, for instance, J. Wilks, *The Properties of Liquid and Solid Helium* (Clarendon, Oxford, England, 1967), Chap. 3.
[57]These results are similar to the values $\zeta = 0.677 \pm 0.02$, $y = 0.36 \pm 0.1$ quoted in our preliminary publications Refs. 22 and 23. The preliminary values resulted from a single least-squares fit of all of the data with $\epsilon < 10^{-2}$, and depended on the adequacy of simple polynomials in P to describe the amplitudes k and a. We prefer to present values of ζ and y which do not depend on this unnecessary assumption.

PHYSICAL REVIEW A VOLUME 7, NUMBER 6 JUNE 1973

Generality of the Uniform-Limit Formalism for Many-Boson Systems in the Weak-Coupling Limit*†

Deok Kyo Lee
Department of Physics and Astronomy, University of Kansas, Lawrence, Kansas 66044
(Received 23 June 1971; revised manuscript received 12 February 1973)

Ground states of two typical many-boson model systems are studied: (i) a weakly interacting boson system at low density, and (ii) a low-density hard-sphere boson gas in the low-energy limit. For both of these systems it is shown explicitly that the uniform-limit formalism based on the method of correlated basis functions can be used to obtain, in a relatively simple way, exact results for the ground-state energy per particle and other related properties in the weak-coupling limit. In the problem of the hard-sphere boson gas the T-matrix method is found to be particularly useful in dealing with the singular interaction potential.

I. INTRODUCTION

A wide variety of microscopic theories have recently been developed for various types of interacting many-particle boson systems to investigate low-temperature properties associated with the ground state and low-lying excited states. In particular, quite extensive use has been made of the formal perturbation theory based on systematic application of the Feynman diagrammatic techniques in the second-quantization space. Although this approach is no doubt very powerful, it suffers from the disadvantage that nearly all such many-body perturbation series involve divergencies which must be removed one way or another to obtain physically meaningful results. On the other hand, variational approaches have also been shown to be very useful and sometimes more elegant than the formal perturbation method since the troublesome divergencies do not usually appear in the variational calculations.

One of the well-known variational wave functions for the ground state is the Bijl–Dingle–Jastrow (BDJ) type of trial form,[1-3] i.e., a symmetric